

Measurement of Flow Velocity and Inference of Liquid Viscosity in a Microfluidic Channel by Fluorescence Photobleaching

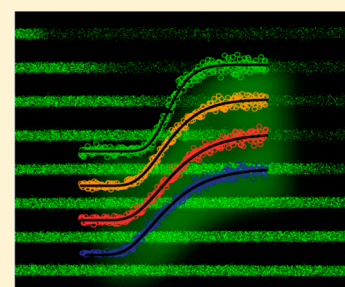
Nick J. Carroll,^{†,‡} Kaare H. Jensen,^{†,§,#} Shima Parsa,[‡] N. Michele Holbrook,[§] and David A. Weitz^{*,‡}

[‡]School of Engineering and Applied Sciences and Department of Physics, Harvard University, 29 Oxford Street, Cambridge, Massachusetts 02138, United States

[§]Department of Organismic and Evolutionary Biology, Harvard University, 16 Divinity Avenue, Cambridge, Massachusetts 02138, United States

[#]Department of Physics, Technical University of Denmark, Kongens Lyngby DK-2800, Denmark

ABSTRACT: We present a simple, noninvasive method for simultaneous measurement of flow velocity and inference of liquid viscosity in a microfluidic channel. We track the dynamics of a sharp front of photobleached fluorescent dye using a confocal microscope and measure the intensity at a single point downstream of the initial front position. We fit an exact solution of the advection diffusion equation to the fluorescence intensity recovery curve to determine the average flow velocity and the diffusion coefficient of the tracer dye. The dye diffusivity is correlated to solute concentration to infer rheological properties of the liquid. This technique provides a simple method for simultaneous elucidation of flow velocity and liquid viscosity in microchannels.



INTRODUCTION

An important challenge in biological and synthetic microfluidic systems is simultaneous measurement of liquid viscosity and flow velocity when limited by a small liquid volume. The utility of noninvasive fluidic measurements is of considerable importance for determining transport within micro- and nanochannels and living tissues, including the capillary vasculatures of plants¹ and animals.² The Venturi- and Pitot tube method,³ hot-wire anemometry,⁴ laser Doppler velocimetry,⁵ and particle image velocimetry⁶ are robust techniques used to measure the velocity in fluid flows. However, in most micro- or nanofluidic systems, these classical techniques cannot easily be applied, either because the channel volume is too small or because the measurement would disrupt the flow. This happens, for example, when the size of a tracer particle approaches that of the channel under investigation.⁷ Additionally, these techniques do not provide a simple process for simultaneous elucidation of physical properties such as solute concentration or fluid viscosity.

Alternatively, recent advances in fluorescent-microscopy-based techniques have facilitated noninvasive measurement of both flow velocity and liquid properties within various micro- and nanofluidic systems. For example, analysis of fluorescence recovery after photobleaching (FRAP) has been used to measure the flow velocity in lymphatic capillaries of mice⁸ and in straight or curved microchannels.^{9,10} In addition to velocity measurements, FRAP analysis is an effective method for quantifying fluidic properties by elucidation of fluorescent dye diffusivity; for instance, static 1-D diffusion measurements of a carefully loaded fluorescent analyte plug were demonstrated within fluidic channels.¹¹ Perhaps the most powerful feature of FRAP-based fluidic measurements in biological and synthetic

systems is the versatility to measure both average fluid velocity and dye diffusion simultaneously. Elegant theoretical techniques were developed to quantify convective and diffusive transport and determine their contributions to fluorescence recovery in an infused liquid medium.¹² The fundamental methodology of these techniques entails tracking the temporal evolution of a well-defined photobleached front and subsequent fitting of the digitized fluorescence intensity data to a solution of the advection–diffusion equation.¹³ This adaptable approach has been used to determine dye diffusivity and fluid velocity in micro-⁹ and nanochannels^{14,15} and within the microenvironment of animal tissue.² A challenge of these FRAP techniques, however, is they require precise tracking of a photobleached front throughout the entire region of interest and multiple time-dependent curve-fits to characterize diffusive and convective effects. Additionally, commonly used Gaussian function curve-fitting relies on well-defined photobleached geometries; this demand places constraints on the laser beam profile, thus requiring specific optical components for precise focusing of the beam into the sample. The utility of FRAP for measurement of flow velocity and liquid composition for practical application could be further extended by simplification of previous methods; thus, a less demanding approach for elucidation of convective and diffusive transport properties remains an important yet unmet need.

We have developed a simple, noninvasive FRAP technique for simultaneous measurement of flow velocity and fluorescent dye diffusivity in a microfluidic channel. We use confocal

Received: December 20, 2013

Revised: March 22, 2014

Published: March 23, 2014

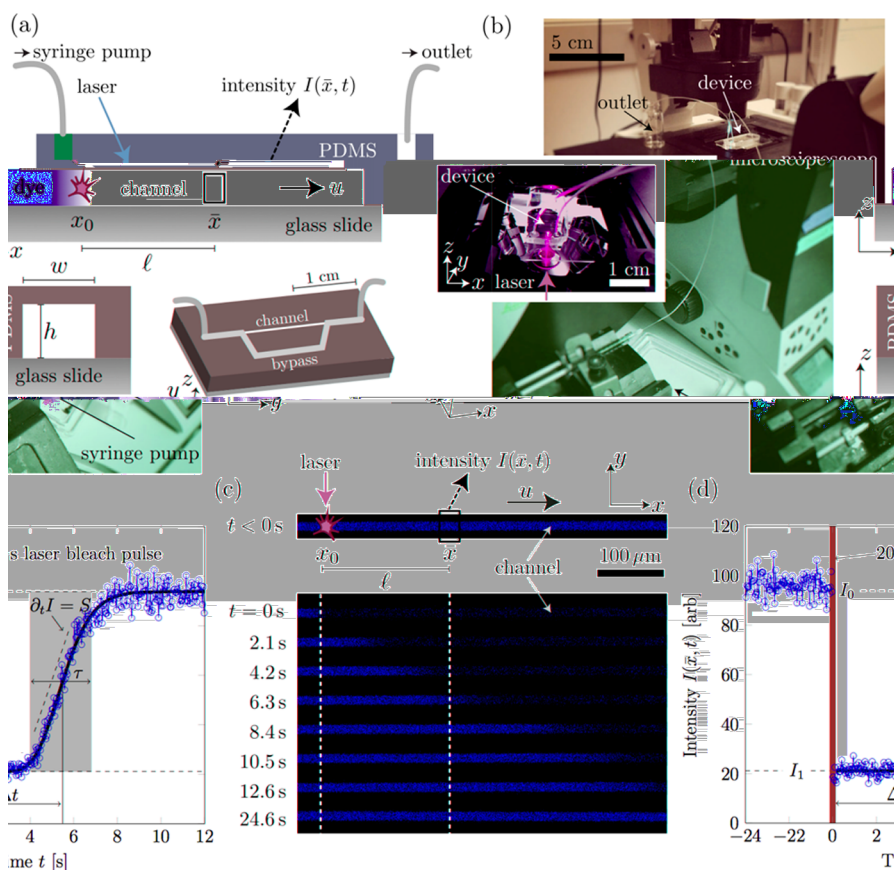


Figure 1. Experimental setup and data processing. (a) Schematic of the experimental setup. A syringe pump drives a flow of average speed $u = 15\text{--}150\ \mu\text{m/s}$ in a microfluidic channel of height $h = 10\ \mu\text{m}$, width $w = 10\ \mu\text{m}$, and length $L = 1\ \text{cm}$. To obtain steady liquid motion at low flow rates, a bypass channel measuring $105\ \mu\text{m} \times 105\ \mu\text{m} \times 2\ \text{cm}$ was used to divert the bulk of the volumetric flow delivered by the syringe pump. (b) Photograph of the experimental setup showing the device mounted in the inverted confocal microscope. Inset shows a close-up of the device with laser illumination from below. (c) Image sequence illustrating a characteristic experiment. Initially, the fluorescent dye present in the channel is bleached for 20 s by an intense laser beam point focused at position x_0 . When the laser is turned off (at time $t = 0$), the fluorescent intensity is recorded by the confocal microscope as a function of time in a region measuring $20\ \mu\text{m} \times 510\ \mu\text{m}$ (40×1024 pixel). The front of dye, initially located at x_0 , is advected along the x -axis while it broadens due to diffusion. To quantify the advection and diffusion of the fluorescent dye, we measure the average intensity $I(\bar{x}, t)$ as a function of time t in a small $5\ \mu\text{m} \times 10\ \mu\text{m}$ region centered at the position $\bar{x} = x_0 + l$. (d) Intensity $I(\bar{x}, t)$ plotted as a function of time t for a $c = 40\%$ wt sucrose solution driven with a pump speed of $u \approx 35\ \mu\text{m/s}$. Having traveled a distance $l = 180\ \mu\text{m}$, the front arrives at the region of interest after $\Delta t = 5.5\ \text{s}$. The transition in intensity between the bleached level I_1 and the unbleached I_0 takes $\tau \approx 2.8\ \text{s}$ (gray region). The solid black line shows a least-squares fit to the intensity curve predicted by eq 6 with fitted velocity $u = 32\ \mu\text{m/s}$ and diffusivity $D = 103\ \mu\text{m}^2/\text{s}$. From the scaling results in eqs 1 and 3, we estimate the flow speed $u = l/\Delta t = 33\ \mu\text{m/s}$ and dye diffusivity $D = 1/(4\pi)(\tau/l/\Delta t^{3/2})^2 = 122\ \mu\text{m}^2/\text{s}$, in rough accord with the values determined from the curve fit.

microscopy to quantify the advection and diffusion of a molecular dye by measuring the average fluorescence intensity as a function of time in a small $5\ \mu\text{m} \times 10\ \mu\text{m}$ region downstream of a laser bleach point. We acquire a fluorescence recovery profile from which the average flow speed and fluorescent dye diffusivity are elucidated by a least-squares fit of the advection–diffusion equation to the experimentally obtained sigmoid-shaped recovery curve. Furthermore, we correlate dye diffusivity with solute concentration to infer the viscosities for a number of aqueous sugar and polymeric solutions. Particle tracking velocimetry (PTV) is used to measure the average fluid velocities at different flow rates to corroborate the fluid velocities obtained using our FRAP technique. Determining both velocity and dye diffusivity from a single fluorescence recovery curve obviates the need for tracking well-defined photobleached geometries throughout the entire region of interest; thus, our technique simplifies previous photobleaching approaches and has potential for

application in both synthetic and biological microfluidic systems.

EXPERIMENTAL SECTION

Microfluidics. We flow aqueous solutions of sucrose (Sigma-Aldrich, 342.30 g/mol) or polyethylene glycol (PEG) (Sigma-Aldrich, 3500 g/mol) and the fluorescent dye carboxyfluorescein (CF, AnaSpec Inc., 376.32 g/mol) through a long, straight, rectangular microfluidic channel. The channel length $L \approx 1\ \text{cm}$ is much greater than the channel width $w = 10\ \mu\text{m}$ and height $h = 10\ \mu\text{m}$. The microchannel was fabricated in polydimethylsiloxane (PDMS) and bonded to a microscope slide using standard soft lithography techniques.¹⁶ A CF dye concentration of $10\ \mu\text{M}$ was used throughout. To maximize the fluorescent intensity of the CF dye, the pH of each solution was adjusted to ~ 9 by adding small amounts of potassium hydroxide (KOH). In the following, the term solute refers to sucrose or PEG. A schematic sketch of the device and a photograph of the setup are shown in parts a and b of Figure 1, respectively. We control the flow speed in the channel by connecting the device to a syringe pump (Harvard Apparatus PHD 2000). At the channel outlet the solution

flows into a reservoir kept at atmospheric pressure. The flow speed u is varied over an order of magnitude, $u = 15\text{--}150\ \mu\text{m/s}$, and the solute concentration is in the range $c = 0\text{--}40\%$ wt for sucrose and $c = 0\text{--}20\%$ wt for PEG; see Table 1. A total of 163 experiments were performed

Table 1. Diffusion Coefficient D and Viscosity η Determined As Described in the Text; Results Given for Aqueous Solutions of Carboxyfluorescein (CF) and a Solute (Sucrose or PEG) of Concentration c ; Values Obtained at Temperature $T = 20\ ^\circ\text{C}$ with Pump Flow Rates in the Range $50\text{--}100\ \mu\text{L}/\text{min}$

solution	c (% wt)	η (mPa s)	D ($\mu\text{m}^2/\text{s}$)
water + CF		1.002 ²⁸	444 \pm 61
water + CF + sucrose	10	1.30 \pm 0.02	301 \pm 25
water + CF + sucrose	20	1.75 \pm 0.06	230 \pm 21
water + CF + sucrose	40	5.01 \pm 0.03	94 \pm 11
water + CF + PEG	5	4.08 \pm 0.05	263 \pm 63
water + CF + PEG	10	10.90 \pm 0.06	189 \pm 42
water + CF + PEG	15	26.0 \pm 0.2	159 \pm 18
water + CF + PEG	20	55.6 \pm 0.3	118 \pm 13
Diet Coca-Cola	0		414 \pm 82
Coca-Cola	10.5		281 \pm 55
Red Bull	10.5		249 \pm 75
A&W Cream Soda	12.5		208 \pm 69
water + CF			487 \pm 22 ²⁹
water + fluorescein			425 \pm 1 ³⁰

with at least 3 repetitions for each combination of flow rate and concentration. Further experiments were conducted using four different commercially available liquids containing sucrose (soft drinks); see Table 1. These were degassed using a vacuum chamber, and the pH was adjusted as described previously using KOH.

Viscosity Measurements. The viscosities of the aqueous sugar and polymeric solutions are measured using a strain-controlled rheometer (TA ARES G2) with parallel-plate geometry.

Particle Tracking. We use particle tracking velocimetry (PTV) to measure the average fluid velocities in the channel at different pump flow rates to calibrate the dye tracking technique. The fluid is seeded with $0.5\ \mu\text{m}$ diameter fluorescent carboxylate microsphere tracer particles (Invitrogen) at a low seeding density ($\phi = 5 \times 10^{+5}\ \text{mL}^{-1}$) to avoid particle–particle interactions. We image an area of $510 \times 20\ \mu\text{m}^2$ ($1024 \times 40\ \text{pixel}^2$) at frame rates between 22.2 and 7.7 Hz depending on the imposed flow rate. The center of the particles are identified to an accuracy of 1/3 of a pixel ($0.2\ \mu\text{m}$). The particle velocities are then measured as the time derivative of the measured

particle trajectories. The velocity profile is measured at the middle plane of the channel from at least 25 000 successful velocity samples. We then fit the experimentally measured velocity profile to the solution for the rectangular channel flow profile of a square microchannel¹⁷ to determine the flow speed, u , in the channel.

Fluorescence Photobleaching. We use a confocal microscope (Leica Microsystems GmbH, Wetzlar, Germany; scan time $s = 41\ \text{ms}$) with a $10\times$ dry objective lens (numerical aperture 0.3) to acquire single-channel fluorescence images. For this, we use an argon (458 nm) laser as the excitation and photobleaching source of the CF dye; the fluorescence emission is collected by the photomultiplier (PMT) detector through bandpass filters between 460 and 530 nm. A conventional optical microscope could be used in similar experiments, for example, by switching to a higher magnification during the bleaching phase. We apply fluorescence photobleaching with the goal of measuring the flow speed u , solute concentration c , and solution viscosity η . We first bleach the fluorescent dye in part of the channel and subsequently monitor the dynamics of the fluorescent dye as it is advected by the flow while undergoing molecular diffusion as exemplified by the image sequence in Figure 1c. To ensure that we are only observing the dynamics of mobile dye not bound to the channel walls, we perform the bleaching by focusing a laser beam at the channel position $x = x_0$ for a bleaching time of $t_b = 20\ \text{s}$. Because the liquid is moving at an average speed of u set by the syringe pump, the intense laser pulse renders most of the dye in the channel between x_0 and $x_1 = x_0 + ut_b$ inert and thereby unable to fluoresce. This reduces the fluorescent intensity in the bleached region from the initial level I_0 , proportional to the dye concentration, to the level $I_1 < I_0$. After the laser is powered off, we monitor the dynamics of the fluorescent dye using confocal microscopy, as shown in Figure 1c, d. To quantify the dye dynamics, we record the fluorescence intensity $I(\bar{x}, t)$ as a function of time t at the observation position \bar{x} , shown in Figure 1d.¹⁸ We average the intensity measured at \bar{x} over a $(x, y, z) = 5 \times 10 \times 10\ \mu\text{m}^3$ volume. The $5\ \mu\text{m}$ width along the x -direction gave a good signal-to-noise ratio, and although it is comparable to the initial front width ($\sim 10\ \mu\text{m}$), it is 10–20 times smaller than the width observed during the intensity transition. In the following, we choose the time $t = 0$ to coincide with the laser being turned off. For $t > 0$, we observe that the fluorescent intensity at \bar{x} varies between I_1 and the prebleach constant level I_0 . This is due to the combined effect of liquid flow (convection), which carries unbleached dye toward the observation region and facilitates Taylor-Aris dispersion, and molecular diffusion, which broadens the boundary between the bleached and unbleached regions, initially located at x_0 . Acting together, these effects lead to a sigmoid-shaped transition between the two intensity levels, as shown in Figure 1d.

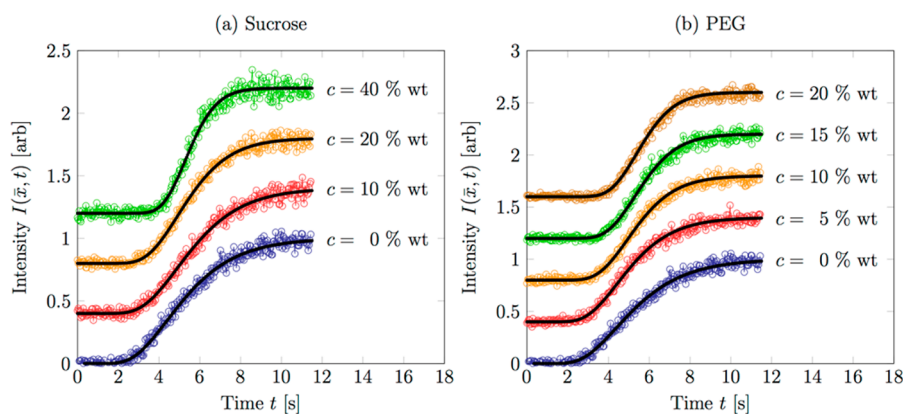


Figure 2. Experimental data. Examples of observed fluorescent intensity $I(\bar{x}, t)$ (open circles) plotted as a function of time t for (a) sucrose and (b) PEG solutions flowing at a speed of $u = 35\ \mu\text{m/s}$. The solute concentration c is indicated next to the data curves. Solid black lines are least-squares fits to eq 3 with two free parameters: the dye diffusivity D and the flow velocity u .

RESULTS AND DISCUSSION

Analysis. Figure 2 shows a series of characteristic fluorescent intensity curves observed in our experiments. The solute concentration increases from bottom to top. We note the general trend that increasing the solute concentration leads to growth in the slope of the intensity curves in the transition region highlighted by the gray area in Figure 1d. The effect of increasing the flow velocity is to shift the curves to the left. To elucidate how the flow speed u , solute concentration c , and solution viscosity η can be determined from recovery curves as those shown in Figure 2, we analyze the dynamics of the dye in the channel. As demonstrated by numerous experimental and theoretical studies,^{19,20} there is a strong correlation between the diffusion coefficient D of the dye and the bulk viscosity η of the solution. For incompressible Newtonian fluids at constant temperature, the viscosity is determined primarily by the solute concentration c . With proper viscosity and flow calibration measurements, quantitative knowledge of the diffusivity D will thus allow us to infer the solute concentration c and the viscosity η of simple fluids.

The flow speed u and the dye diffusivity D are obtained from our experiments using a single fit to an exact solution of the advection–diffusion equation. To elucidate the dominant transport mechanisms, however, we begin by giving a scaling argument demonstrating how u and D are determined. See ref 21 for a more detailed account of nonlinear dispersion phenomena. Under our experimental conditions, the motion of dye is approximately one-dimensional and occurs primarily along the x -direction. This approximation is justified by comparing the time scales for diffusion in the transverse (y, z)-plane of the channel $\tau_{yz} = w^2/D \approx 0.1$ s with the time scale for advection along the x -direction $\tau_x = l/u \approx 1$ –10 s. Here, $l = \bar{x} - x_0$ is the distance between the observation point \bar{x} and the laser bleach position x_0 .

We approximate the flow speed u by

$$u = \frac{l}{\Delta t} \quad (1)$$

where Δt is the time from when the laser is turned off until the dye front arrives at \bar{x} , having traveled the distance l . Assuming an initially sharp front, the arrival time Δt is the point when the observed intensity reaches half its maximum value, i.e., when $I(\bar{x}, \Delta t) = (I_0 + I_1)/2$, as indicated in Figure 1d.

We proceed to derive an expression for the diffusivity D . The observed apparent value of the diffusivity D_{eff} may differ from the true value D due to Taylor-Aris dispersion, which augments the dispersion along the flow direction. The origin of the enhanced spreading is related to velocity variations in the direction transverse to the mean flow.^{22–24} Because of this effect, the observed apparent diffusivity D_{eff} is larger than the true value D by an amount $D_{\text{eff}} = D(1 + \gamma Pe^2)$, where $Pe = uh/D$ is the Péclet number and the constant $\gamma = 0.0084$ for a square channel.²⁴ Our experiments are performed at Péclet numbers in the range $Pe \approx 0.1$ –5, and the observed diffusivity can thus be up to 20% greater than the true value. We correct for this effect in the subsequent analysis but continue to use the symbol D for the diffusivity corrected for Taylor-Aris dispersion effects. We note that ballistic dispersion dominates at short times compared to the transverse diffusion time $\tau_{yz} \approx 0.1$ s (see, e.g., ref 21), but we do not include this explicitly in our analysis.

To elucidate how we deduce the diffusivity D from the experimental data, we consider the characteristic slope $S = (I_0 -$

$I_1)/\tau = \Delta I/\tau$ of the intensity curve during the sigmoid transition between the intensity levels I_1 and I_0 over the time τ as shown in Figure 1d. The transition time scale τ is naturally related to the front width a and the flow speed u by $\tau \approx a/u$. The front width $a(t)$ increases with time due to molecular diffusion; thus, to a first approximation, we can write $a(t) \approx a_0 + (kDt)^{1/2}$, where a_0 is the initial front width and k is a constant determined by the channel geometry and the initial conditions. The front width a becomes several times greater than the initial value $a_0 \approx 10$ μm over the course of a few seconds as evidenced by Figure 1c; hence, in the following we assume that $a(t) = (kDt)^{1/2}$. With these assumptions, we arrive at an expression for the slope S :

$$S = \frac{\Delta I}{\tau} = \frac{\Delta I u}{(kD\Delta t)^{1/2}} = \frac{\Delta I l}{(kD\Delta t)^{1/2} \Delta t} \quad (2)$$

Equation 2 allows us to determine the diffusivity D in terms of the slope S and the remaining parameters:

$$D = \frac{1}{k} \left(\frac{\Delta I l}{S \Delta t^{3/2}} \right)^2 = \frac{1}{k} \left(\frac{\tau l}{\Delta t^{3/2}} \right)^2 \quad (3)$$

To improve on the estimates for u and D given in eqs 1 and 3, and to determine the numerical value of the constant k , we proceed to consider the dye motion as described by the one-dimensional advection–diffusion equation: $\partial_t c + u \partial_x c = D \partial_x^2 c$. We assume that the observed intensity I is proportional to the dye concentration c , in which case the equation of motion for the fluorescent intensity is

$$\partial_t I + u \partial_x I = D \partial_x^2 I \quad (4)$$

We use a step function centered at $x = x_0$ to describe the initial condition at $t = 0$, c.f., Figure 1c,

$$I(x, t = 0) = \begin{cases} I_0 & \text{for } x < x_0 \\ I_1 & \text{for } x > x_0 \end{cases} \quad (5)$$

The solution to eqs 4 and 5 can be found using standard techniques¹⁷ and is given by

$$I(\bar{x}, t) = I_1 + \frac{I_0 - I_1}{2} \left[1 - \text{erf} \left(\frac{l - ut}{(4Dt)^{1/2}} \right) \right] \quad (6)$$

where $l = \bar{x} - x_0$ is the distance from the bleach point to the observation region. From a fit to the experimental data, we can thus determine the dye diffusivity D and flow speed u from a single fluorescence recovery curve. Our computational algorithm for analyzing the experimental data used the `fminsearch` implementation of the Nelder-Mead unconstrained nonlinear optimization method in MATLAB (The MathWorks, Inc., version 2011a). We return briefly to the scaling analysis, which leads to eq 3. To determine the constant k in eq 3, we compute the characteristic slope S of the recovery curve from the exact solution in eq 6 evaluated when the center of the front is at $x = \bar{x}$, i.e., at $t = l/u$:

$$S = \left. \frac{\partial I}{\partial t} \right|_{t=l/u} = \frac{\Delta I u}{(4\pi D l/u)^{1/2}} \quad (7)$$

such that $k = 4\pi$.

Comparison between Experiment and Theory. Representative intensity curves obtained in our experiments are compared to the functional form of eq 6 in Figure 2. Each curve

fit has two free parameters, representing the diffusivity D of the dye and the flow speed u . We find good qualitative agreement between the shape of the observed intensity profiles and eq 6. The flow speed u derived using our method is compared to results obtained with particle tracking in Figure 3a with

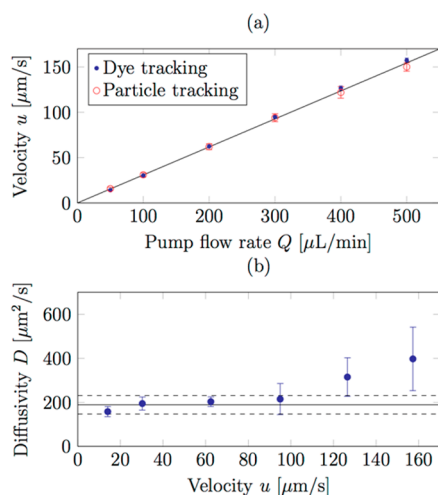


Figure 3. Calibration measurements. (a) Flow velocity u determined by fitting intensity recovery curves to eq 6 (dots) and from particle tracking experiments (circles) plotted as a function of syringe pump flow rate Q . (b) Diffusivity D determined from fitting intensity recovery curves to eq 6 plotted as a function of flow velocity u . Solid and dashed lines show diffusivity mean \pm standard deviation obtained at flow speeds less than $u = 100 \mu\text{m/s}$. The values shown in (a) and (b) were obtained using a 10% PEG solution. Error bars indicate standard deviation.

excellent correspondence between the two. The diffusivity D obtained with our technique is shown as a function of flow speed u in Figure 3b. Below the speed $u = 100 \mu\text{m/s}$, there is relatively little variation in the inferred diffusivity. At higher velocities, however, both the value of the diffusivity and the uncertainty in the measurement increases rapidly. We attribute this trend to two effects. First, when the flow speed u increases, the time $\tau = a/u$ for the diffusive front of width a to pass through the detection region decreases. Given that the image

acquisition time $s = 41 \text{ ms}$ is constant in our experiments, the number of data points in the transition region $N \approx \tau/s$ decreases. Second, because we use a point laser to bleach the fluorescent dye while it is flowing past position x_0 , we naturally decrease the laser power deposited in a given fluid volume per unit time when increasing the flow speed. This implies that, at high speeds, the relative difference between the two intensity levels I_0 and I_1 will be smaller than those at low speeds where the time to bleach is longer. Both these circumstances affect the data fit because they determine how accurately the slope S of the intensity curve can be measured, c.f., eq 3. Our experiments suggest that approximately $N \approx 100$ data points are needed in the transition region to determine the diffusivity D accurately. To minimize experimental error in a given application, the laser scan time s and the observation position \bar{x} must thus be tailored accordingly.

We proceed to discuss results obtained at flow speeds at or below $u = 100 \mu\text{m/s}$. Figure 4 shows the correlation between the derived dye diffusivity and the solute concentration (panel a and b) and solution viscosity (panel c). We observe that increasing the solute concentration and viscosity leads to a decrease in the dye diffusivity. The character of this correlation has been investigated previously in numerous theoretical and experimental studies.^{19,20,26,27} By balancing thermal drift and viscous drag on the dye molecule, one arrives at the Stokes–Einstein relation,

$$D = \frac{k_B T}{6\pi\eta r} \quad (8)$$

where k_B is Boltzmann's constant, T is absolute temperature, η is the bulk viscosity of the solution, and r is the effective hydrodynamic radius of the dye molecule.¹⁹ Equation 8 can be presumed to be valid when the dye molecules are much larger than the solvent (water) and solute (sucrose, PEG) molecules, i.e., when $M_{\text{dye}}/M_{\text{solvent}} \gg 1$ and $M_{\text{dye}}/M_{\text{solute}} \gg 1$. These inequalities suggest that the theory may apply to sucrose ($M_{\text{dye}}/M_{\text{solvent}} \approx 21$, $M_{\text{dye}}/M_{\text{solute}} \approx 1.1$) but not to PEG ($M_{\text{dye}}/M_{\text{solvent}} \approx 21$, $M_{\text{dye}}/M_{\text{solute}} \approx 0.1$) where deviations from eq 8 are expected. Encounters between dye and solute molecules are rare in this limit, and dye molecules will thus primarily experience viscous drag from solvent molecules. This implies

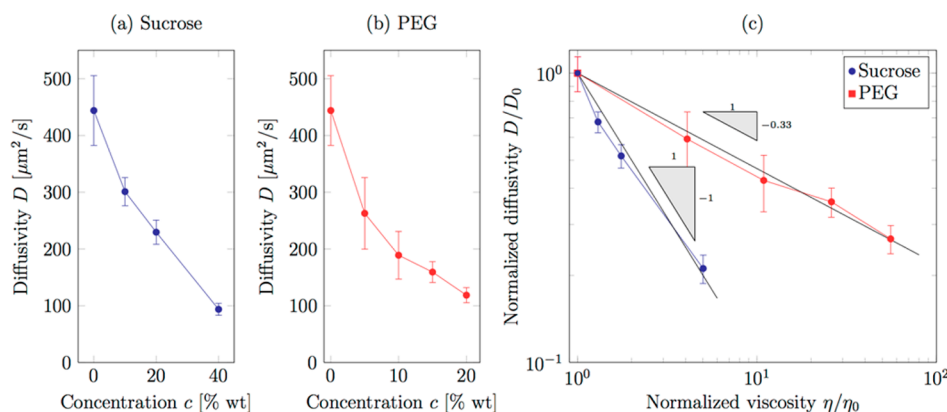


Figure 4. Dye diffusivity D determined from fits to eq 6 plotted as a function of solute concentration c for (a) sucrose and (b) PEG solutions. Data for the pump flow rates 50–300 $\mu\text{L/min}$ are shown. Examples of curve fits are shown in Figure 2. (c) Double logarithmic plot of the normalized diffusivity D/D_0 as a function of the solution bulk viscosity η/η_0 where the subscript indicates values for pure water. Results for the dilute sucrose concentrations are in rough accord with Stokes–Einstein relation ($D \approx \eta^{-1}$; see text), while the dye diffusivity decays slower ($D \approx \eta^{-0.33}$) for the PEG solutions. Error bars indicate standard deviation.

that the diffusivity D should decay slower as a function of the bulk viscosity η than predicted by eq 8 when $M_{\text{dye}}/M_{\text{solute}} \ll 1$.

To test the predictions of eq 8, we measured the viscosity of the aqueous solutions using a rheometer with parallel-plate geometry. The solutions behaved as constant-viscosity Newtonian fluids in the range of shear rates relevant to our experiments (10–100/s). For the aqueous sucrose solutions, there is reasonable agreement between the experimental results and the $D \approx \eta^{-1}$ scaling predicted by eq 8 (see Figure 4c). Note that the diffusivity has been corrected for Taylor-Aris effects. Small deviations are expected because the criteria for eq 8 are only approximately satisfied. For the aqueous PEG solutions, we find significant deviations from eq 8 and estimate that for this system $D \approx \eta^{-0.33}$. As discussed above, this inconsistency with the Stokes–Einstein relation is not surprising given the large difference in size between the solvent and dye molecules. For both the PEG and the sucrose solutions, however, we observe a strong correlation between the dye diffusivity and the solute concentration. This indicates that, with proper calibration measurements, our technique can be used to determine the composition and viscosity of an otherwise unknown liquid flowing in a microfluidic channel. To further demonstrate this, we measured dye diffusion in four different commercially available liquids: Coca-Cola, Diet Coca-Cola, A&W Cream Soda, and Red Bull. These liquids contain sugars of unknown composition in mass concentrations of 0–12.5%; see Table 1. The dye diffusivities obtained from these liquids are consistent with values obtained from pure sucrose solutions, although consistently lower. We attribute this to the presence of additional solutes, which may effectively increase the concentration, and to liquid evaporation during degassing.

In summary, our approach provides a reproducible method for determining the flow velocity u and the dye diffusivity D over a wide range of solutions and channel flow speeds. From these, we are able to infer solute concentration and liquid viscosity.

CONCLUSIONS

We introduce a simple, noninvasive method for simultaneous measurement of flow velocity and liquid viscosity in a microfluidic channel. The flow speed is determined by tracking a front of photobleached fluorescent dye while the viscosity is inferred by correlating it with observations of the diffusion coefficient of the dye. Both velocity and diffusivity are determined from a single fit to an exact solution of the advection–diffusion equation. Elucidation of both velocity and diffusivity from a single fluorescence recovery curve eliminates the requirement of well-defined photobleached geometries; this simplification of previous FRAP methods obviates the need for complex optical components and multiple time-dependent curve fitting. Scaling results are given to elucidate the important experimental factors in determining these parameters. We perform experiments using sucrose and polyethylene glycol solutions to elucidate a strong negative correlation between the dye diffusivity and the bulk viscosity of the solution; we rationalize these observations based on the Stokes–Einstein relation. Particle tracking velocimetry is used to corroborate the average fluid velocities at different flow rates obtained using our FRAP technique. We further apply our method to determine the sugar content of four different commercially available soft drinks liquids.

AUTHOR INFORMATION

Corresponding Author

*E-mail: weitz@seas.harvard.edu.

Author Contributions

†These authors contributed equally to this work.

Notes

The authors declare no competing financial interest.

ACKNOWLEDGMENTS

The authors wish to thank M. Knoblauch, S. Beecher, J. Savage, and D. Froelich for useful discussions. We also thank Jing Fan for kindly assisting in the viscosity measurements. This work was supported by the NSF (Grant no. 1021779), the Materials Research Science and Engineering Center at Harvard University (MRSEC, NSF Grant no. DMR-0820484), and the Air Force Office of Scientific Research (Award no. FA9550-09-1-0188).

REFERENCES

- (1) Froelich, D. R.; Mullendore, D. L.; Jensen, K. H.; Ross-Elliott, T. J.; Anstead, J. A.; Thompson, G. A.; Pelissier, H. C.; Knoblauch, M. Phloem ultrastructure and pressure flow: Sieve-element-occlusion-related agglomerations do not affect translocation. *Plant Cell* **2011**, *23*, 4428–4445.
- (2) Chary, S. R.; Jain, R. K. Direct measurement of interstitial convection and diffusion of albumin in normal and neoplastic tissues by fluorescence photobleaching. *Proc. Natl. Acad. Sci. U. S. A.* **1989**, *86*, 5385–5389.
- (3) Bailey, S. C. C.; Hultmark, M.; Monty, J. P.; Alfredsson, P. H.; Chong, M. S.; Duncan, R. D.; Fransson, J. H. M.; Hutchins, N.; Marusic, I.; McKeon, B. J.; Nagib, H. M.; Orlu, R.; Segalini, A.; Smits, A. J.; Vinuesa, R. Obtaining accurate mean velocity measurements in high Reynolds number turbulent boundary layers using pitot tubes. *J. Fluid Mech.* **2013**, *715*, 642–670.
- (4) Molki, A.; Khezzi, L.; Goharzadeh, A. Measurement of fluid velocity development in laminar pipe flow using laser Doppler velocimetry. *Eur. J. Phys.* **2013**, *34*, 1127–1134.
- (5) Konig, J.; Voigt, A.; Buttner, L.; Czarske, J. Precise micro flow rate measurements by a laser Doppler velocity profile sensor with time division multiplexing. *Meas. Sci. Technol.* **2010**, *21*.
- (6) Devasenathipathy, S.; Santiago, J. G.; Wereley, S. T.; Meinhart, C. D.; Takehara, K. Particle imaging techniques for microfabricated fluidic systems. *Exp. Fluids* **2003**, *34*, 504–514.
- (7) Pouya, S.; Koochesfahani, M. M.; Greytak, A. B.; Bawendi, M. G.; Nocera, D. G. Experimental evidence of diffusion-induced bias in near-wall velocimetry using quantum dot measurements. *Exp. Fluids* **2008**, *44*, 1035–1038.
- (8) Berk, D. A.; Swartz, M. A.; Leu, A. J.; Jain, R. K. Transport in lymphatic capillaries. 2. Microscopic velocity measurement with fluorescence photobleaching. *Am. J. Physiol.: Heart Circ. Physiol.* **1996**, *270*, H330–H337.
- (9) Mosier, B. P.; Molho, J. I.; Santiago, J. G. Photobleached-fluorescence imaging of microflows. *Exp. Fluids* **2002**, *33*, 545–554.
- (10) Wang, G. R. Laser induced fluorescence photobleaching anemometer for microfluidic devices. *Lab Chip* **2005**, *5*, 450–456.
- (11) Pappaert, K.; Biesemans, J.; Clicq, D.; Vankrunkelsven, S.; Desmet, G. Measurements of diffusion coefficients in 1-D micro- and nanochannels using shear-driven flows. *Lab Chip* **2005**, *5*, 1104–1110.
- (12) Chary, S. R.; Jain, R. K. Analysis of diffusive and convective recovery of fluorescence after photobleaching-effect of uniform-flow field. *Chem. Eng. Commun.* **1987**, *55*, 235–249.
- (13) Jain, R. K.; Stock, R. J.; Chary, S. R.; Rueter, M. Convection and diffusion measurements using fluorescence recovery after photobleaching and video image analysis: in vitro calibration and assessment. *Microvasc. Res.* **1990**, *39*, 77–93.

- (14) Cuenca, A.; Bodiguel, H. Fluorescence photobleaching to evaluate flow velocity and hydrodynamic dispersion in nanoslits. *Lab Chip* **2012**, *12*, 1672–1679.
- (15) Cuenca, A.; Bodiguel, H. Submicron flow of polymer solutions: Slippage reduction due to confinement. *Phys. Rev. Lett.* **2013**, *110*, 108304.
- (16) Xia, Y. N.; Whitesides, G. M. Soft lithography. *Angew. Chem., Int. Ed.* **1998**, *37*, 551–575.
- (17) Bruus, H. Theoretical microfluidics; OUP: Oxford, U.K., 2008.
- (18) The position \bar{x} is chosen to be located between the laser bleach at x_0 and the middle of the bleached region, i.e., at $x_0 \leq \bar{x} \leq (x_0 + x_1)/2$. Although our analysis works for any value of \bar{x} between x_0 and x_1 , having a relatively large separation between \bar{x} and x_1 allows us later to disregard the diffusion of dye into the observation region from the front initially located upstream at x_1 .
- (19) Bird, R. B.; Stewart, W. E.; Lightfoot, E. N. *Transport phenomena*; Wiley: New York, 2007.
- (20) Brillo, J.; Pommrich, A. I.; Meyer, A. Relation between self-diffusion and viscosity in dense liquids: New experimental results from electrostatic levitation. *Phys. Rev. Lett.* **2011**, *107*.
- (21) Frankel, I.; Brenner, H. On the foundations of generalized Taylor dispersion theory. *J. Fluid Mech.* **1989**, *204*, 97–119.
- (22) Ajdari, A.; Bontoux, N.; Stone, H. A. Hydrodynamic dispersion in shallow microchannels: The effect of cross-sectional shape. *Anal. Chem.* **2006**, *78*, 387–392.
- (23) Aris, R. On the dispersion of a solute in a fluid flowing through a tube. *Proc. R. Soc. London, Ser. A* **1956**, *235*, 67–77.
- (24) Taylor, G. Dispersion of soluble matter in solvent flowing slowly through a tube. *Proc. R. Soc. London, Ser. A* **1953**, *219*, 186–203.
- (25) Datta, S.; Ghosal, S. Characterizing dispersion in microfluidic channels. *Lab Chip* **2009**, *9*, 2537–2550.
- (26) Einstein, A. Über die von der molekularkinetischen theorie der wärme geforderte bewegung von in ruhenden flüssigkeiten suspendierten teilchen. *Ann. Phys.* **1905**, *322*, 549–560.
- (27) Edward, J. T. Molecular volumes and the Stokes–Einstein equation. *J. Chem. Educ.* **1970**, *47*, 261.
- (28) Haynes, W. M. L. D. R. *CRC Handbook of Chemistry and Physics: A ready reference book of chemical and physical data*; CRC Press: Boca Raton, FL, 2011.
- (29) Kramer, E. M.; Frazer, N. L.; Baskin, T. I. Measurement of diffusion within the cell wall in living roots of *Arabidopsis thaliana*. *J. Exp. Bot.* **2007**, *58*, 3005–3015.
- (30) Culbertson, C. T.; Jacobson, S. C.; Ramsey, J. M. Diffusion coefficient measurements in microfluidic devices. *Talanta* **2002**, *56*, 365–373.